Retrievals of water vapour and temperature exploiting the far-infrared: application to aircraft observations in preparation for the FORUM mission

Sanjeevani Panditharatne[1-3], Helen Brindley[1,3], Caroline Cox[2], Richard Siddans[2,4], Jonathan Murray[1,3], Laura Warwick[5], and Stuart Fox[6]

[1]Imperial College London, London, UK
[2]RAL Space, Harwell Oxford, Chilton, UK
[3]NERC National Centre for Earth Observation, Imperial College London, London, UK
[4]NERC National Centre for Earth Observation, RAL Space, Harwell Oxford, Chilton, UK
[5]ESA-ESTEC, Noordwijk, The Netherlands
[6]Met Office, Exeter, UK

Correspondence: Sanjeevani Panditharatne (s.panditharatne21@imperial.ac.uk)

Abstract.

We present the extension of the RAL Infrared Microwave Sounding (IMS) optimal estimation retrieval scheme to include the use of far-infrared channels in preparation for the upcoming Far-infrared Outgoing Radiation Understanding and Monitoring (FORUM) mission. The IMS code has been previously applied to mid-infrared spectral radiances measured by the Infrared Atmospheric Sounding Instrument (IASI) to retrieve temperature and water vapour. Given this, the evolution and evaluation of the extended scheme is performed in two steps. First, clear-sky retrievals of temperature and water vapour are performed on IASI and FORUM simulations. Comparable retrieval biases are observed for retrievals of temperature and water vapour, however there is an increase of ∼1 degree of freedom for water vapour and temperature for the FORUM configuration. Secondly, radiances observed from an aircraft flight in the upper troposphere are modified to match the FORUM spectral characteristics. Retrievals from these radiances using the modified code show a strong agreement with contemporaneous in-situ measurements of the atmospheric state, reducing the RMSE by 18% for water vapour from the a-priori, giving confidence in its performance. The extended IMS scheme is now available for use on FORUM observations and can be easily adapted to other far and mid-infrared instrument configurations.

1 Introduction

Water vapour composes approximately 3% of the Earth's atmosphere and is the most dominant greenhouse gas with absorption bands in the microwave, infrared, and visible spectral regions (Harries, 1996; Andrews, 2000). Capturing its spatial and temporal distribution is critical in quantifying the Earth's greenhouse effect, characterising atmospheric circulation, and approximating the strength of water vapour's radiative effect and feedback which has the potential to exacerbate anthropogenic climate change (Dessler et al., 2008; Chung et al., 2014).

20   Water vapour in the upper troposphere strongly regulates this water vapour feedback (Chung et al., 2014), with current increases in tropospheric moisture consistent with an amplifying water vapour feedback (IPCC, 2023). However, discrepancies in long-term trends exist between observations, climate models, and reanalysis datasets (Schröder et al., 2019; Santer et al., 2021; Allan et al., 2022). Considerable work has been performed to improve assessments of water vapour distributions through the use of in-situ measurements such as radiosondes and aircraft-based sensors (Sun et al., 2021). However, best-case uncertainties

25   from the GCOS Reference Upper Air Network (GRUAN) radiosondes are estimated to still be of the order 5%, reaching 15% near the tropopause (Dirksen et al., 2014), with limited homogeneity in the radiosondes' distribution, regularity, and vertical sampling (Ferreira et al., 2019).

Satellite observations across the electromagnetic spectrum have also been used to characterise the atmosphere with increased spatial coverage. However, satellite retrievals can lack sufficient vertical resolution (Chung et al., 2014), demonstrate an in-

30   herent bias (Santer et al., 2021), or have a reduced sensitivity to UT water vapour (Kursinski and Gebhardt, 2014) causing inconsistencies between retrieved upper tropospheric humidities (Shi et al., 2022). While hyperspectral sounders such as Atmospheric Infrared Sounder (AIRS), and the Infrared Atmospheric Sounding Interferometer (IASI) have improved the vertical resolution of water vapour and temperature (Chahine et al., 2006; Hilton et al., 2012), radiances in the mid-infrared (667-2000 cm^{-1}) have a limited sensitivity to water vapour in the mid to upper troposphere, and upper tropospheric biases remain present

35   (Fetzer et al., 2008; Trent et al., 2019).

In the global mean, the far-infrared region (100-667 cm^{-1}) accounts for approximately 55% of the outgoing longwave radiation (OLR) and the absorption of water vapour dominates this region, with its pure rotational band extending from 6-667 cm^{-1} (Brindley and Harries, 1998). As a consequence, radiances in this region are significantly more sensitive to mid and upper tropospheric water vapour than in the mid-infrared (Sinha and Harries, 1995; Brindley and Harries, 1998).

40   Due to technical limitations, there are historically no observations of spectrally resolved far-infrared radiances at the top of the atmosphere (TOA). This is changing, with space missions such as NASA's Polar Radiant Energy in the Far-InfraRed Experiment and ESA's Far-infrared Outgoing Radiation Understanding and Monitoring (FORUM) mission, the former having launched in summer 2024, and the latter scheduled for launch in 2027 (L'Ecuyer et al., 2021; Palchetti et al., 2020).

This study is in support of the FORUM mission which aims to measure the Earth's spectrally resolved OLR using the

45   FORUM Sounding Instrument (FSI), which will have a spectral range from 100-1600 cm^{-1} with a spectral resolution greater than 0.5 cm^{-1} and a target radiometric accuracy of 0.1 K at 3σ. The FORUM satellite will fly in a loose formation with the EUMETSAT MetOp-SG-1A satellite, complementing mid-infrared observations of the OLR taken by the Infrared Atmospheric Sounding Instrument New Generation (IASI-NG), and when combined will create a unique dataset of the Earth's entire OLR spectrum (Palchetti et al., 2020).

50   Given the sensitivities and spectral features across the far-infrared for water vapour, there is a significant potential for improved retrievals from the upcoming TOA observations in the far-infrared (Harries et al., 2008; Ridolfi et al., 2020). Theoretical studies by Merrelli and Turner (2012) demonstrated this potential in retrievals of simulated upwelling radiances with realistic instrument configurations, and the benefit of far-infrared information has recently been confirmed by Warwick et al. (2022) who performed a single retrieval on a spectrum covering the far- and mid-infrared observed from an aircraft flying in the upper

troposphere. To date, other existing retrieval codes built to exploit the far-infrared have only been tested on simulations of upwelling far and mid-infrared radiances, and observations of downwelling radiances limited to the spectral range 200-1000 cm^{-1} (Di Natale et al., 2020; Ridolfi et al., 2020).

This paper presents the extension of the RAL Infrared Microwave Sounding retrieval scheme for the upcoming FORUM mission into the far-infrared, focusing on clear-sky retrievals of water vapour and temperature using the optimal estimation method. It is a fast and flexible retrieval code that has been built to perform multi-target retrievals of instruments onboard the MetOp satellites covering the mid-infrared and microwave spectral regions. It can simultaneously retrieve several atmospheric and surface components (Siddans et al., 2017), including cloud properties, and its ability to retrieve temperature and water vapour profiles using the mid-infrared has been thoroughly evaluated in Siddans (2019) and Trent et al. (2023).

To test this scheme in the far-infrared, it has undergone two stages of testing. The first is an assessment of the retrieval performance on a diverse set of simulations of upwelling radiances at the top of the atmosphere, exploiting the entire FSI spectral range. The second builds on the earlier work of Warwick et al. (2022) by adapting aircraft-based observations to mimic the expected FSI instrumental characteristics, developing what we term FORUM-aircraft radiances. We also include a greater number of radiometric observations from the flight and optimise the IMS channel selection for the FORUM-aircraft configuration. The retrieval performance of the extended IMS code applied to these FORUM-aircraft observations is then evaluated through comparison with contemporaneous in-situ atmospheric measurements.

The layout of the paper is as follows: in Section 2 we outline the retrieval scheme and methodology. Section 3 details the extension for FORUM and Section 4 outlines the testing on simulated cases. Section 5 describes the aircraft campaign and observations. Section 6 outlines modifications made to the retrieval framework and the observations to improve their representation of the FORUM Sounding Instrument. Section 7 contains the final retrievals from observations, with conclusions in Section 8

2 Retrieval Framework

The RAL Infrared Microwave Sounding (IMS) retrieval scheme uses the optimal estimation method to simultaneously retrieve vertical profiles of atmospheric temperature and gases, along with surface skin temperature, surface spectral emissivity and cloud parameters (Rodgers, 2000; Siddans, 2019). It was initially developed for joint retrievals of observations from IASI as well as the Microwave Humidity Sounder (MHS), and the Advanced Microwave Sounding Unit (AMSU) on the MetOp satellites for retrievals of the vertical methane profile, and is a customisable retrieval framework that can be easily adapted to a variety of other instruments. As part of the ESA Water Vapour Climate Change Initiative project, Trent et al. (2023) evaluated the IMS water vapour and temperature retrieval products from IASI observations across a 9.5 year period against two sets of radiosonde measurements. A mean global water vapour bias of 10% and temperature bias within 1 K were seen between retrieved profiles and radiosonde measurements.

A brief overview of the optimal estimation method used within IMS is outlined below, however full details of the IMS algorithm can be found in Siddans (2019) and Trent et al. (2023). IMS uses the optimal estimation method from Rodgers

(2000) to fit an observed spectrum (the measurement vector, $\mathbf{y}$) by iteratively perturbing the retrieval targets (the state vector, $\mathbf{x}$). Estimations of $\mathbf{y}$ are calculated from adjusted values of $\mathbf{x}$ using a forward model, $\mathbf{F}(\mathbf{x})$, which in this case is a radiative transfer model. Prior knowledge of the state is contained in the a-priori state vector, $\mathbf{x}_a$, with covariance, $\mathbf{S}_a$, representing the vertical variability and correlation of the profile, and both are used to constrain the retrieval. Similarly, the measurement covariance, $\mathbf{S_y}$, represents the uncertainty in the measurement, and for IASI has been calculated based on the residual between simulations and bias-corrected IASI observations in the current IMS configuration (Trent et al., 2023).

The Radiative Transfer for TOVS v12 (RTTOVv12) fast radiative transfer model is used as the forward model in the IMS scheme. It can simulate clear-sky and cloudy spectra with atmospheric profiles input onto 101 fixed pressure levels using coefficients to increase its operational speed (Haiden et al., 2018). These coefficients are derived by performing a regression on a database of transmittances of atmospheric gases calculated from the top of the atmosphere to each fixed pressure level using the Line-By-Line Radiative Transfer Model v12.8 (LBLRTMv12.8) (Clough et al., 2005), for all the profiles in the European Centre for Medium-Range Weather Forecasts (ECMWF) diverse 83-profile dataset that was developed to capture a large variety of atmospheric states (Chevallier et al., 2006). The LBLRTM transmittances include the effects of 28 gas species, alongside continua (MT_CKDv3.2) due to water vapour (self- and foreign broadening), ozone, carbon dioxide, nitrogen, and oxygen (Saunders et al., 2017). They are adapted to match the instrument line shape of ∼90 different satellite sensors, and so each set of regression coefficients is customised to the specific instrument (Haiden et al., 2018; Saunders et al., 2017).

In this work, we perform simultaneous retrievals of temperature (K), water vapour (ppmv), surface skin temperature (K), and surface emissivity. We use hourly ERA-5 reanalysis data as the a-priori for temperature, water vapour and surface skin temperatures rather than the climatology used in Trent et al. (2023) as a tighter constraint given the limited number of observations of far-infrared radiances. Vertical profiles for CO_2, O_3, CH_4, N_2, and other trace gases are fixed to the US 1976 Standard profile unless specified otherwise. The a-priori for surface emissivity is taken from the IREMIS surface emissivity atlas within RTTOVv12 (Seeman et al., 2008). This uses the input latitude, longitude and snow fraction for land to determine the surface emissivity based on an offline database. For sea, the emissivity is parameterised in terms of zenith angle, wind speed and skin temperature and calculated offline based on refractive indices from Hale and Querry (1973), and a wave slope model from Masuda (2006). The a-priori covariance for temperature, water vapour and skin temperature is a 2-dimensional matrix derived from the differences between the zonal mean of ERA-5 profiles for three days (17 April, 17 July, and 17 October 2013). The a-priori covariance for the surface emissivity is derived from surface emissivities from the IREMIS atlas for the same time period. Both of these covariance matrices contain correlations manifested as non-zero off-diagonal elements.

2.1 Retrieval Method

Iterations are based on the Levenburg-Marquardt (LM) method (Marquardt, 1963):

$$\mathbf{x}_{i+1} = \mathbf{x}_i + \left(\mathbf{K}_i^T \mathbf{S_y}^{-1} \mathbf{K} + \mathbf{S}_a^{-1} + \gamma_i\right)^{-1} \left[\mathbf{K}_i^T \mathbf{S_y}^{-1} \left(\mathbf{y} - \mathbf{F}\left(\mathbf{x}_i\right)\right) - \mathbf{S}_a^{-1}\left(\mathbf{x}_i - \mathbf{x}_a\right)\right] \tag{1}$$

where i is the iteration, γ is the LM parameter controlling the magnitude of the state vector perturbation and is initially set to 0.001 in IMS, and $\mathbf{K}_i$ is a Jacobian matrix of partial derivatives of the forward model output to elements of the state vector.

The fit optimisation is based on minimising the cost, χ^2, with the first and second terms on the right-hand side of equation 2 corresponding to the measurement and state cost, respectively:

$$\chi^2 = (\mathbf{y} - \mathbf{F}(\mathbf{x}))^T \mathbf{S_y}^{-1} (\mathbf{y} - \mathbf{F}(\mathbf{x})) + (\mathbf{x} - \mathbf{x}_a)^T \mathbf{S}_a^{-1} (\mathbf{x} - \mathbf{x}_a) \tag{2}$$

The measurement cost indicates the fit of the simulated and observed spectra in relation to the $\mathbf{S_y}$ in the selected channels. A larger measurement cost per channel indicates a worse fit and suggests that the retrieved state vector is less likely to match the true state. The state cost indicates how far the retrieved state has deviated from the a-priori in relation to $\mathbf{S}_a$. A high state cost could be caused by either an a-priori which is not similar to the true state, or a small $\mathbf{S}_a$, which suggests the retrieval is tightly constrained.

The retrieval is performed using selected channels rather than for the entire spectral range to minimise operational time and eliminate unreliable channels. It is said to have converged when χ^2 has reduced, is the lowest value calculated so far, and the change in χ^2 is less than 1. If the cost increases but is below a set threshold, the retrieval stops based on a low cost. If 10 iterations are reached and the criteria have not been met, the retrieval has not converged. These settings can be varied and have been optimised based on retrievals from IASI observations.

Several other metrics are used to assess the performance of the retrieval. The first is the covariance of the retrieved state, $\mathbf{S}_x$, which is the covariance of a Gaussian probability distribution function:

$$\mathbf{S}_x = (\mathbf{S}_a^{-1} + \mathbf{K}^T \mathbf{S_y}^{-1} \mathbf{K})^{-1} \tag{3}$$

where the square root of the diagonal of this matrix represents the error in the retrieved state and is equivalent to one standard deviation. This will be referred to as the estimated standard deviation (ESD) in the retrieval.

The second is the averaging kernel (AK) matrix, $\mathbf{A}$, that represents the vertical sensitivity of the retrieved to the true state. A larger averaging kernel means a greater amount of the retrieval is from the observation rather than the a-priori. This is, in practice, calculated using the gain matrix, $\mathbf{G}$ which is the sensitivity of the retrieval to the measurement and its uncertainty, and can be used to smooth a true state, $\hat{\mathbf{x}}$, to the resolution of the retrieval:

$$\mathbf{A} = \frac{\partial \hat{\mathbf{x}}}{\partial \mathbf{x}} = \mathbf{GK} \tag{4}$$

The third parameter is the degrees of freedom for signal (DOFS) which represents the number of independent pieces of information and is calculated from the trace of $\mathbf{A}$.

The final parameter is the root mean squared error (RMSE) value which is calculated using the difference between the a-priori or retrieved profile and the true profile. The RMSE values for water vapour are calculated using the units of the logarithm of

specific humidity as concentrations can vary by several orders of magnitude throughout the vertical, and are used as a summary value to further assess the quality of the retrieval.

 ## 3 Extension of IMS for FORUM

When developing the IMS retrieval scheme for use on FSI observations, the first thing to consider is the ability of the forward model to simulate spectra. The RTTOVv12 regression coefficients used to simulate spectra have already been built for the FSI and can be easily integrated into the retrieval framework. The RTTOVv12 FSI radiances cover the full FSI spectral range at a sampling of 0.3 cm^{-1} and have the strong Norton-Beer apodisation applied. This results in a total of 5000 channels and a spectral resolution of 0.6 cm^{-1}. This necessitates two key modifications to the retrieval process. The first is the adjustment of spectrally varying covariance matrices used to constrain the retrieval (Section 3.1). The second is the selection of channels to optimise the spectral fitting performed in the retrieval (Section 3.2).

3.1 Covariance Adaptions

The a-priori covariance for the surface emissivity and measurement covariance are both spectrally dependent and so must be tailored to the specifications of the FSI defined in RTTOVv12. They are currently configured for the mid-infrared and microwave spectral regions with spectral sampling and ranges for instruments on board the MetOp satellites. Both of these correlated covariance matrices can be found in the supplementary information.

The surface emissivity is also retrieved as its been shown to improve the agreement between retrievals of lower tropospheric water vapour and ECMWF analyses, as well as reducing cloud contamination (Trent et al., 2023). The same method as described in Section 2 was used to calculate the a-priori covariance for sea cases and extend it to the far-infrared. For land cases, the surface emissivity produced by the IREMIS atlas is fixed in the far-infrared, and so the covariance was instead found using an emissivity database that covers the FSI spectral range (Huang et al., 2016).

The measurement covariance was built using the apodised target noise-equivalent-spectral-radiances (NESR) and target absolute radiometric accuracy (ARA) for the FSI. These two components have been combined to produce a correlated covariance matrix. The leading diagonal of the matrix is shown in Figure 1b. It has been separated into the NESR and ARA components in Figure 1c with the full matrix included in Figure S2 in the supplementary information. The apodised NESR includes four sets of non-zero off-diagonals due to the thin instrument line shape and is the dominant contributor to the measurement covariance below 1300 cm^{-1} and above 1450 cm^{-1}. The target ARA is 0.1 K between 300 and 1100 cm^{-1}, 0.2 K between 200 and 300 cm^{-1} and 1100 and 1300 cm^{-1}, and 1K elsewhere. As the ARA is defined in brightness temperature, it is converted into radiance units for each individual spectrum, and the average is shown in Figure 1c for the ECMWF 83-profiles. We assume that the ARA covariance is fully correlated, and so it has contributions off the leading diagonal of up to 0.5 $[\text{mWm}^{-2}\text{sr}^{-1}/\text{cm}^{-1}]^2$ below 100 cm^{-1} and above 1300 cm^{-1}.

This measurement covariance relates to the FSI 15km footprint and acquisition time of 8s. The leading diagonal of the IASI measurement covariance outlined in Section 2 is shown in Figure 1a. This corresponds to the IASI 12 km footprint which also
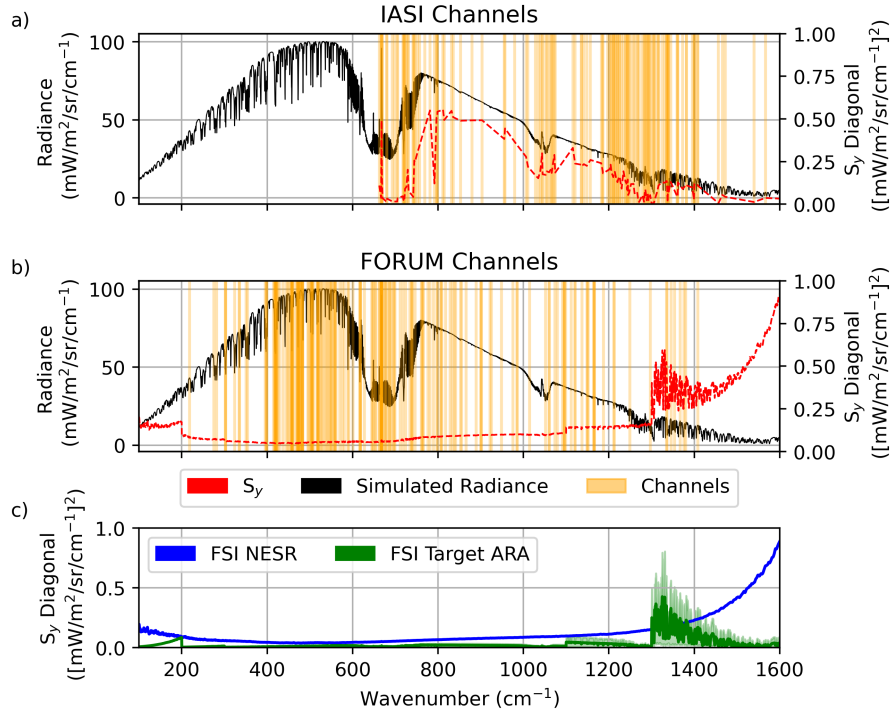
Figure 1. An example upwelling FORUM spectrum simulated using RTTOVv12 overplotted with channels selected for (a) IASI and (b) FORUM retrievals. The main diagonal of the measurement covariance $\mathbf{S_y}$ is shown in red in both cases. (c) The main diagonal of the FORUM measurement covariance separated into components from the noise-equivalent-spectral-radiance (NESR) and the target absolute radiometric accuracy (ARA). As the ARA is provided in brightness temperature, it has been converted into radiance units for each of the ECMWF 83 profiles. The median is shown here, with the shading representing the minimum and maximum values.

180 has an acquisition time of 8s. As can be deduced from Figure 1, the FSI measurement covariance is between 0.08 and 0.37 $[\mathrm{mWm^{-2}sr^{-1}/cm^{-1}}]^2$ smaller than its IASI counterpart between 750 and 1200 $\mathrm{cm^{-1}}$. At wavenumbers above 1300 $\mathrm{cm^{-1}}$, the FSI measurement covariance increases, reaching a difference of 0.9 $[\mathrm{mWm^{-2}sr^{-1}/cm^{-1}}]^2$ at 1600 $\mathrm{cm^{-1}}$.

3.2 Channel Selection

IMS uses 139 out of the available 8460 IASI channels (Figure 1a), each with a channel width of 0.25 $\mathrm{cm^{-1}}$ and a spectral
185 resolution of 0.5 $\mathrm{cm^{-1}}$ (Trent et al., 2023). These were selected to maximise the information content of the retrieval for temperature, water vapour, and ozone, as well as filtering channels for noise and reliability. Final channels were added or removed to enhance the retrieval outputs for these profiles on an ad-hoc basis for general retrievals from IASI observations. (Collard, 2007; Watson, 2011).

A similar analysis is performed here for the channel selection for the FSI. The 5000 channels available for FORUM are
190 ranked based on their contribution to the total available information content for the ECMWF diverse 83-profile set (Chevallier

et al., 2006). The parameter for information content, **H**, is dependent on the sensitvity of the retrieval to the measurement and a-priori covariance, and is calculated using equation 5 by exploiting **A** outlined in equation 4 (Rodgers, 2000),

$$\mathbf{H} = -\frac{1}{2}\ln|\mathbf{I} - \mathbf{A}| \tag{5}$$

where **I** is an identity matrix.

Therefore, **H** can be used to filter out channels with a greater uncertainty and weaker sensitivity to the retrieval products. In this case, the a-priori covariance is a weak constraint and so the measurement covariance plays a more significant role in the channel selection.

Improvements in the information content and DOFS for temperature and water vapour plateaued for the FORUM configuration at 200 channels, with no notable improvements when more channels were included. Therefore, these 200 channels have been selected for use in IMS for the FORUM configuration, and are shown in Figure 1b. These capture ∼66% of the total available information content, with the remaining channels each contributing at most 0.1%. Unlike the IASI case in Figure 1a, no channels are selected at wavenumbers greater than 1400 cm^{-1}. Similarly, no channels below 200 cm^{-1} are selected. A markedly reduced percentage of channels are located between 1000-1400 cm^{-1} in comparison to the IASI selection as the noise characteristics associated with the FSI have effectively shifted the locations of peak information to the range 400-700 cm^{-1} for water vapour, and information relating to ozone (and other trace gases) has not been prioritised.

4 Simulated Test Cases

Given the limited number of observations of upwelling TOA radiances in the far-infrared region, preliminary testing was performed using simulated test cases for the IASI and FORUM configurations. The input or 'true' profiles are known for each test case, and as a result, the retrieved products can be compared against the truth without any introduction of uncertainty in the atmospheric state. The ability of IMS to retrieve from IASI observations is well documented, and so we use this as a reference output to assess the performance of the updated FORUM configuration.

A number of existing artificial datasets have been crafted to encompass variable atmospheres, such as the ECMWF diverse 83-profile dataset, however, these have already been used in generating the RTTOVv12 coefficients and for the channel selection in Section 3.2 (Saunders et al., 2017). Reanalysis datasets, including but not limited to ERA5 and CAMS, have also been used in the development of IMS and while the reliance of IMS on these datasets is very weak, they do not provide an independent basis for testing IMS (Siddans, 2019). Therefore, we constructed a test set from Modern-Era Retrospective analysis for Research and Applications, Version 2 (MERRA-2) reanalysis data produced by NASA Global Modeling and Assimilation Office (Gelaro et al., 2017). MERRA-2 has been shown to perform comparably to ERA-5 when assessed against observations and is an independent base for this test set (Jiang et al., 2015; Arshad et al., 2021; Huang et al., 2021; Johnston et al., 2021).

Instantaneous 3-hourly MERRA-2 reanalysis data is used for temperature, water vapour, and ozone vertical profiles (Global Modeling and Assimilation Office and Pawson, 2015a). Ozone is not a retrieval target in this work and is fixed to the 'true'
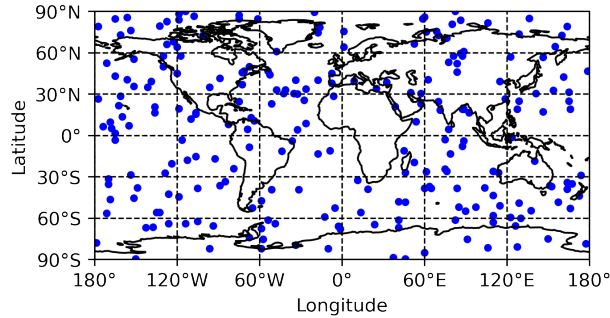
Figure 2. The spatial distribution of the 240 cases selected for testing IMS. Profiles were derived from MERRA-2. Tropical Cases: 70. Mid-Latitude Cases: 95. Arctic Cases: 75.

profile in each retrieval, but it has been chosen to vary across the test cases given its strong absorption in the mid-infrared. Instantaneous hourly MERRA-2 reanalysis data is used for skin temperatures and surface pressures (Global Modeling and Assimilation Office and Pawson, 2015b).

225 The MERRA-2 data was first restricted to the 1st of March, June, September, and December 2019 to cover a broad range of seasons and conditions. From this data, 240 test cases were selected to capture variations in temperature and water vapour near the surface and in the upper troposphere. The spatial distribution of test cases can be seen in Figure 2, and the distribution of skin temperature and total column water vapour in Figure 3. The selected test cases, shown in red, capture the upper and lower limits of the restricted MERRA-2 data, shown in blue, for skin temperature and total column water vapour, however the

230 distribution of test cases have a slightly smaller proportion of cases with a TCWV below $2.5 \ \mathrm{kgm}^{-2}$. Overall, the finalised test cases demonstrate a comparable spread relative to the initially selected MERRA-2 days.

The US 1976 Standard profiles for CO_2, CH_4, and N_2O were scaled to match National Oceanic and Atmospheric Administration (NOAA) flask measurements averaged from 2019 (Saunders et al., 2017; NOAA ESRL GML CCGG Group, 2019a, b, c), and have been kept constant across all the test cases. Realistic surface emissivities were selected based on their

235 MODIS surface type from the IREMIS atlas and residuals between the IREMIS atlas and Huang emissivity database for sea and land respectively (Platnick et al., 2003; Seeman et al., 2008; Huang et al., 2016), and were also retrieved as outlined in Section 3.1.

4.1 Retrievals from Simulations

Retrievals on RTTOVv12 simulations of all 240 tests cases outlined in Section 4 have been performed for both the IASI

240 and FORUM configurations. Details of the temperature and water vapour retrievals using each configuration are presented in this section. The retrievals of surface emissivity and skin temperature can be found in the supplementary information. The performance of the IASI configuration shows comparable retrieval biases to those observed in Trent et al. (2023) from IASI observations, with a mean bias within 12% and 0.3 K for water vapour and temperature retrievals, respectively. These are
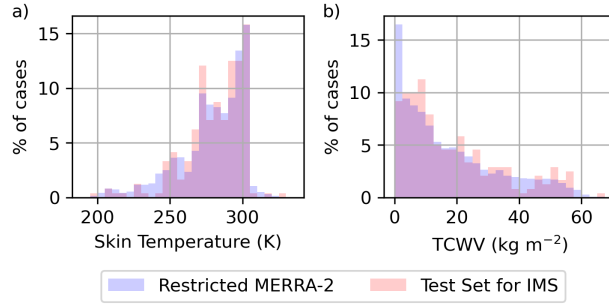
Figure 3. The percentage of total cases with each **(a)** skin temperature, and **(b)** total column water vapour (TCWV) in the MERRA-2 reanalysis dataset for one day in March, June, September, and December in 2019 and used in the test dataset, shown in blue and red respectively. Overlapping regions are shown in purple where the same proportion of cases is present in the test set and MERRA-2 reanalysis dataset.

driven by inherent biases between the a-priori, taken from ERA5, and the MERRA-2 profiles used to simulate the test cases (Johnston et al., 2021).

Table 1 summarises the evaluation metrics for retrievals performed using both the IASI and FORUM configurations. Broadly speaking, the performance of the two configurations is similar, with each metric agreeing within the associated uncertainty seen across the test cases. The FORUM configuration does appear to have a slightly increased state cost, indicative of a greater divergence from the a-priori state, which iterative tests suggest is linked to the addition of information from the far-infrared channels and the channel optimisation in line with findings in (Merrelli and Turner, 2012). It is worth recalling that the FORUM measurement covariance consists solely of the estimated FSI NESR and target calibration uncertainty, while the IASI measurement covariance implicitly also includes forward model error.

The average DOFS for water vapour and temperature were also greater for the FORUM configuration in this comparison, with observed improvements primarily in the upper troposphere. This is shown in the median cumulative degrees of freedom for signal (CDOFS) in Figure 4 which is indicative of the vertical resolution of the retrieved profile. The FORUM configuration (blue) has a sharper increase in the CDOFS between 200 and 400 hPa for both temperature and water vapour. This suggests a slightly higher vertical resolution for the FORUM configuration in the upper troposphere in comparison to the IASI configuration. Below 600 hPa, both configurations have a CDOFS that aligns with a vertical resolution of approximately 200 hPa/DOFS for water vapour and temperature.

The median retrieval biases for both configurations are presented in Figure 5. The FORUM and IASI retrieval configurations perform comparably throughout the vertical, with biases within 2 % and 0.2 K of each other for water vapour and temperature respectively. Generally, the FORUM configuration has a lower median water vapour bias of up to 2%. Between 600 and 700 hPa, the FORUM retrieval does not perform as well, with its water vapour bias reaching up to -2.5%, however this remains within the median estimated standard deviation (ESD) of the retrieval. Noticeably, the ESD associated with the FORUM configuration for water vapour is up to 7% smaller throughout the vertical profile than its IASI counterpart, suggesting a higher

Variable	IASI	FORUM
Water Vapour DOFS	5.0±0.8	5.6±0.8
Temperature DOFS	9.9±0.4	10.4±0.3
Measurement Cost Per Channel	0.06 ± 0.04	0.04 ± 0.01
State Cost	7 ± 2	9 ± 3

Table 1. A summary of the median and median absolute deviation in diagnostic parameters outlined in Section 2.1 for the FORUM retrievals of the 240 test cases for the IASI and FORUM configurations.
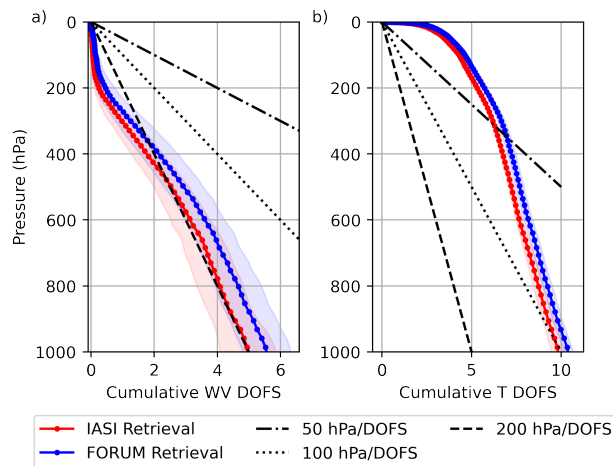
Figure 4. The median cumulative degress of fredom for signal (CDOFS) for **(a)** water vapour and **(b)** temperature averaged across all 240 cases for the IASI and FORUM optimised configurations in red and blue respectively. Shaded regions represent the median absolute deviation. This shows how the vertical distribution of the information content can be related to the vertical resolution of the retrieved profile.

confidence in the retrieved state. However, this is not observed in the temperature retrievals, with the ESD comparable between configurations, and the IASI temperature retrievals performing better above $900\,\mathrm{hPa}$.

5 Observations for Testing

The next stage of testing involves assessing retrievals from aircraft-based observations of upwelling radiances in the far and mid-infrared taken during the PIKNMIX-F campaign. This will highlight limitations in the forward model as well as the wider retrieval framework not explored in the previous section.
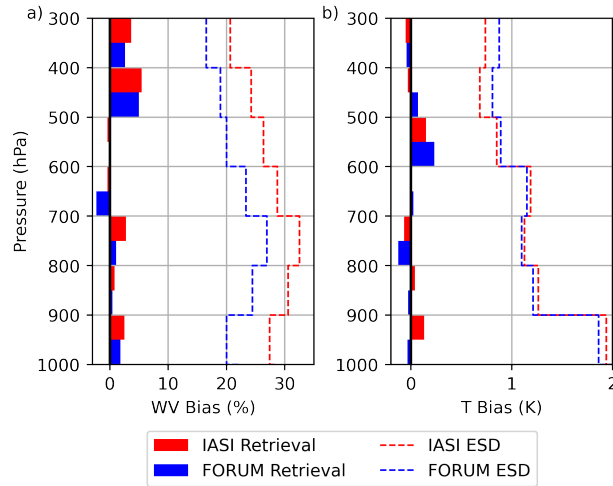
Figure 5. The median **(a)** water vapour (WV) and **(b)** temperature (T) bias of the retrieved profile to the true state across the testing cases for the optimised IASI and FORUM configurations in red and blue respectively. Biases are evaluated between 300 and 1000 hPa in 100 hPa bins as in Trent et al. (2023). The water vapour percentage bias is calculated from absolute values in ppmv. Dashed lines show the median estimated standard deviation (ESD) for a single retrieval for the test cases in each bin. For water vapour this is plotted with an offset of - 10% for clarity.
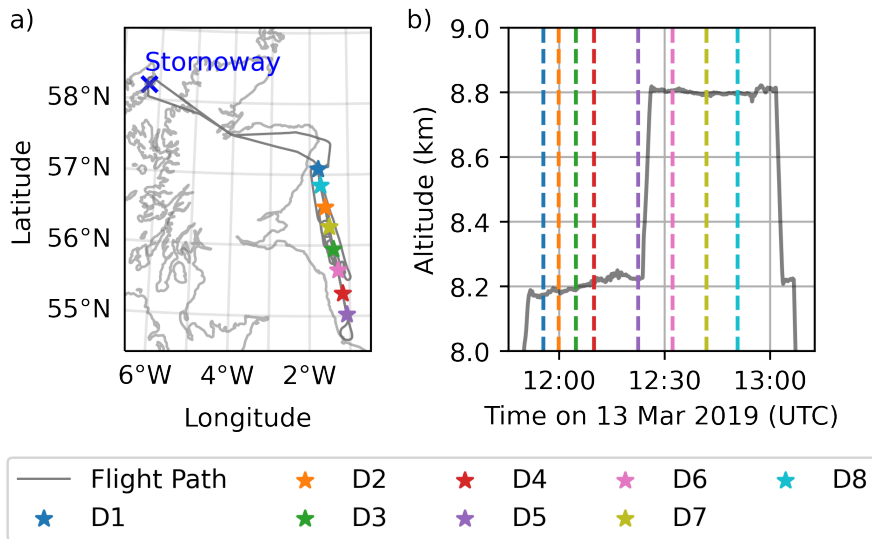
Figure 6. (a) The track of the C153 flight. (b) The altitude measured by the aircraft during the SLRs. Dropsonde releases are marked on (a) and correspond to the dashed lines in (b).

5.1 Flight C153 Overview

The PIKNMIX-F campaign took place in March 2019, based out of Stornoway, Scotland and was a joint venture between the UK Met Office and FAAM Airborne Laboratory. The primary science goals were to obtain data that could be used to improve the representation of specific cloud-microphysical and boundary layer processes within the Met Office suite of models, and to validate radiative transfer modeling of cloudy scenes. Additional funding from ESA allowed further flight hours in support of the FORUM mission, such as the C153 flight that occurred on 13th March 2019.

The C153 flight path and altitude variation are shown in Figure 6. This flight aimed to observe simultaneous nadir-viewing spectra in the far and mid-infrared using the Tropospheric Airborne Fourier Transform Spectrometer (TAFTS) and the Airborne Research Interferometer Evaluation System (ARIES) (Canas et al., 1997; Wilson et al., 1999). Two straight and level runs (SLRs) were conducted between 57 and 55°N from 11:55 to 12:55 UTC at speeds ranging from 175-190 ms^{-1}. The first SLR travelled south-west at an altitude of approximately 8.2km. The aircraft then ascended and flew back over the same path at approximately 8.8km, as highlighted in Figure 6(b). Clear sky conditions were generally observed throughout the flight, with a small amount of low cloud observed near the southern end.

5.1.1 Radiometric Instrumentation

TAFTS is a four port Martin-Puplett interferometer (Canas et al., 1997). Measurements are made at the output ports by pairs of detectors, each containing a "longwave" and "shortwave" detector made of GeGa and SiSb respectively. The instrument has two pairs of blackbody calibration targets held at ambient temperature and 323 K. There is an internal calibration before scans, with a single nadir scan taking $\sim$1.5 s and having an angular field of view of 1.6°. TAFTS has a spectral range of nominally 80-300 cm^{-1} (longwave channel) and 330-600 cm^{-1} (shortwave channel) with a sampling of 0.06 cm^{-1}. It has a nominal spectral resolution of 0.12 cm^{-1}, however, this was reduced to 0.24 cm^{-1}, by reducing the optical path difference and scan time, to reduce the instrument noise and allow more spectra to be collected. The uncertainty on a single TAFTS spectrum is composed of the random noise and calibration error added in quadrature (Figure 8a). In the shortwave channel, this is of the order of $\pm$1-2 mWm^{-2}sr^{-1}/cm^{-1} and in the longwave channel is of the order $\pm$0.5 of mWm^{-2}sr^{-1}/cm^{-1}. In both channels, the uncertainty increases towards the detector band edges.

ARIES uses a Michelson-type configuration with a HgCdTe photodetector for the "longwave" channel and an InSb photodetector for the "shortwave" channel (Wilson et al., 1999). It also has two temperature-controlled blackbody targets and performs periodic calibrations during its measurement sequence. A single ARIES scan takes $\sim$0.25 s and has an angular field of view of 2.5°, with a maximum optical path difference of 1.01 cm. The instrument spectral range covers 550-1800 cm^{-1} (longwave channel) and 1700-3000 cm^{-1} (shortwave channel), with a spectral resolution of 1 cm^{-1} and a spectral sampling of 0.42 cm^{-1}. Only observations from the longwave channel are considered here as the shortwave channel exceeds the FSI spectral range. The ARIES measurement uncertainty also consists of the random noise and calibration error added in quadrature (Figure 8b). Between 650-1350 cm^{-1} this is at most $\pm$1 mWm^{-2}sr^{-1}/cm^{-1} but can reach up to $\pm$4 mWm^{-2}sr^{-1}/cm^{-1} outside of this spectral range.
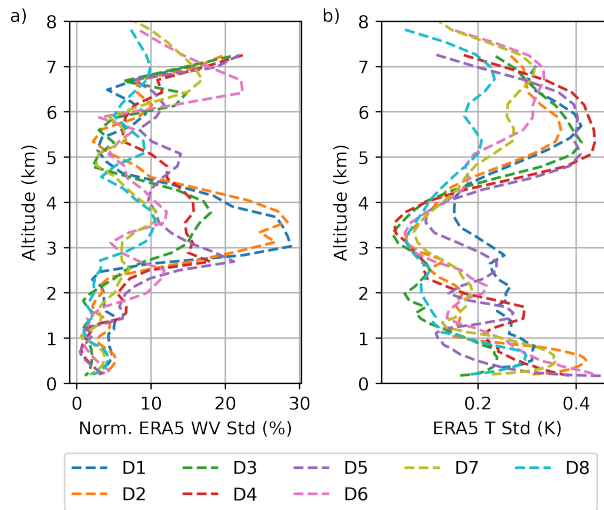
Figure 7. (a) The normalised standard deviation of water vapour (WV) and (b) standard deviation of temperature (T) taken from the ERA5 data surrounding the path of each dropsonde (±30 mins, ±48 km). The spatial resolution of ERA5 is 0.25x0.25° with a temporal resolution of one hour, and thus this plot gives an indication of the variability in the atmosphere at these scales.

5.1.2 Auxiliary Information

On board the FAAM aircraft, additional core instruments have been used to characterise the atmospheric state. Positional information was measured by the POS AV 410 GPS-aided Inertial Navigation unit and static pressure was recorded by the Air Data Computer. Flight level ozone concentrations were recorded by a Core Thermo Fisher Scientific Inc. Model 49i UV absorption ozone photometer. Measurements from the aircraft's spiral descent after the second SLR have been used to build a vertical profile of ozone that is assumed constant throughout the flight and fixed in the retrievals.

The aircraft was also equipped with the Airborne Vertical Atmospheric Profiling System (AVAPS), which released eight Vaisala RD94 dropsondes throughout both SLRs (Figure 6b). Five dropsondes were released during the lower SLR and three during the higher SLR. The Vaisala RD94 dropsondes use the same humidity sensor as the Vaisala RS92 radiosonde, whose uncertainty in humidity measurements was assessed in Miloshevich et al. (2009). The sensor calibration uncertainty was estimated as $\pm5\%$ of the measured relative humidity value plus an absolute offset of $\pm0.5\%$. The production variability uncertainty was $\pm1.5\%$ of relative humidity values above 10% or $\pm3\%$ for values below 10%. No equivalent information is available for the temperature sensor so a manufacturer quoted repeatability of 0.2 K is used to represent the uncertainty.

After release, each dropsonde drifted in a south-westerly direction away from the flight path, remaining within 25 km of their release point. The standard deviation in the ERA5 grid surrounding the path of each dropsonde is shown in Figure 7. Figure 7a suggests a low spatial variability of the water vapour between 4 and 6 km, and below 2km. More variation in ERA5 water vapour is seen between 3 and 4 km, particularly around dropsondes 1 and 2, and above 6 km. Smaller variability is seen in the ERA5 temperature (Figure 7b) around the path of each dropsonde, however, the variation that is present peaks between

Table 2. The times of each dropsonde release and the closest TAFTS scan in time. For each TAFTS scan, the closest 6 ARIES scans are averaged to provide the best match for the field of view and scan time between the instruments. The time of the central ARIES scan is shown.

Dropsonde	Dropsonde Release (UTC)	TAFTS Measurement (UTC)	ARIES Measurement (UTC)
1	11:55:29	11:57:17	11:57:17
2	11:59:53	11:59:43	11:59:42
3	12:04:43	12:04:47	12:04:47
4	12:09:55	12:09:58	12:09:58
5	12:22:27	12:22:23	12:22:22
6	12:32:12	12:32:07	12:32:07
7	12:41:49	12:40:43	12:40:46
8	12:50:39	12:50:39	12:51:07

4 and 8 km and closer to the surface. Given the temporal and spatial resolution of the ERA5 data used (hourly and 0.25x0.25 degrees respectively), this variation can be taken as a lower limit on the in-situ variability that should be considered when evaluating the quality of the retrievals against the dropsonde profiles.

5.2 Selection of Radiance Observations

The dropsondes provide an in-situ measurement of the atmospheric state. Therefore, the TAFTS observation that is closest in time to the release of each dropsonde has been selected. Six ARIES scans centred on each selected TAFTS spectrum were selected to create an average ARIES spectrum which is best matched to the TAFTS' field of view and scan time. This averaging reduces the random component of uncertainty, however, the calibration uncertainty for ARIES tends to be relatively large between 600-1600 cm^{-1}, and so averaging has only a small impact on the total instrument uncertainty.

Final selection times are shown in Table 2. For dropsondes 3-5 and 8, there are observations from TAFTS and ARIES within 5s of the dropsonde release. During the release of dropsonde 8, the ARIES instrument was calibrating and so there is a greater time difference between the TAFTS and ARIES measurements, however ARIES scans in this period are consistent with simulations using the dropsonde 8 profile (Warwick et al., 2022). For dropsonde 2 the TAFTS and ARIES observations are 10s away from the dropsonde release, and for dropsondes 1 and 7 there is over a minute difference which should be considered in later comparisons.

6   Development for Aircraft-Level Retrievals

The coincident aircraft-level observations taken by TAFTS and ARIES present a unique opportunity to assess the potential
340   of what FORUM observations could deliver, as when combined, TAFTS and ARIES cover the full FSI spectral range. To
evaluate this potential, the TAFTS and ARIES observations have been altered to mimic the FSI instrument response function
and spectral sampling, and create 'FORUM-aircraft' observations. Specialised RTTOVv12 transmission coefficients have also
been developed, using LBLRTMv12.11, to enable simulations of upwelling spectra at the altitude of each SLR with the spectral
characteristics of the FSI. This version of LBLRTM uses the MT_CKDv3.5 continuum model, which, most notably for this
345   study, contains an update to the water vapour continuum that increases water vapour absorption within the far-infrared (Mlawer
et al., 2019). A comparison of directly simulated radiances from LBLRTMv12.11 with RTTOVv12 simulations using the
new coefficients typically generated differences that were much smaller than the instrument uncertainty excepting three or
four isolated channels in the far-infrared (Figure 8b) which were subsequently excluded from the channel selection process
described in Section 6.2.
350   This section will focus on evaluating the specialised RTTOVv12 coefficients and adapting the TAFTS and ARIES observa-
tions (Section 6.1), before optimising and testing IMS for this FORUM-aircraft configuration (Section 6.2) on the test cases
from Section 4.

6.1   Constructing FORUM-aircraft observations

The FORUM-aircraft observations are constructed by applying the FSI instrument line shape (ILS) and apodisation to the
355   observed TAFTS and ARIES radiances. Both TAFTS and ARIES each have their own ILS, and TAFTS also has an apodisation
applied to its observed radiances. These cannot be removed, creating a source of error that needs to be quantified to constrain the
retrieval of the FORUM-aircraft observations. To do this, we take the native, high-resolution LBLRTMv12.11 output spectrum
and treat it in two ways. First, we directly apply the FSI ILS and apodisation. Second, we apply the individual TAFTS and
ARIES ILS and apodisation, and then apply the FSI characteristics. By taking the difference between these two methods, we
360   can evaluate the impact of the original instrument characteristics on the FORUM-aircraft measurements.

Figure 8a shows in green that the previous TAFTS spectral characteristics have a minimal effect on radiances over the
majority of the TAFTS spectral range. Closer to the shortwave and longwave detector band edges, this effect increases, however
residuals are predominantly within the measurement uncertainty. In comparison, there is a larger impact on the ARIES spectrum
(Figure 8b) due to its coarser spectral sampling, with residuals often exceeding the measurement uncertainty. This effect is
365   most prominent in the $667 \, \mathrm{cm}^{-1}$ CO_2 band wings which is typically exploited to obtain the vertical temperature profile, and is
likely to degrade the performance of the temperature retrieval. Therefore, the uncertainty caused by the FORUM apodisation
process has been combined with the instrument uncertainty (the dashed lines in Figure 8) in quadrature and together form the
main diagonal of the measurement covariance for the FORUM-aircraft configuration shown in Figure 9.
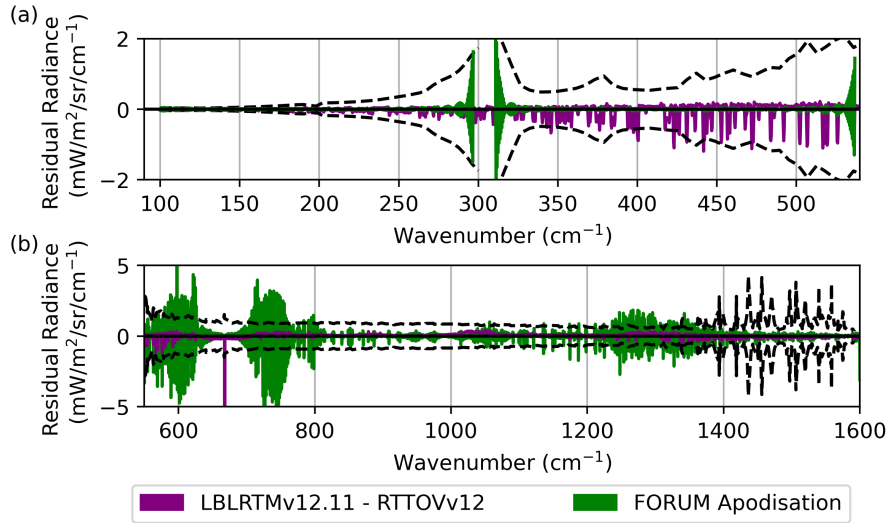
Figure 8. The uncertainty associated with developing FORUM-aircraft observations. The purple line is the residual between an FSI apodised LBLRTMv12.11 simulation and RTTOVv12 FSI simulation using the aircraft-level coefficients in the (a) TAFTS and (b) ARIES spectral ranges. The green line shows the residual between LBLRTMv12.11 simulations of the TAFTS and ARIES observations during the C153 flight that have had the FORUM apodisation directly applied and been made to look like TAFTS or ARIES first as outlined in Section 6.1. The dashed line is the noise and calibration uncertainty combined in quadrature associated with the ARIES LW channel and both TAFTS channels.
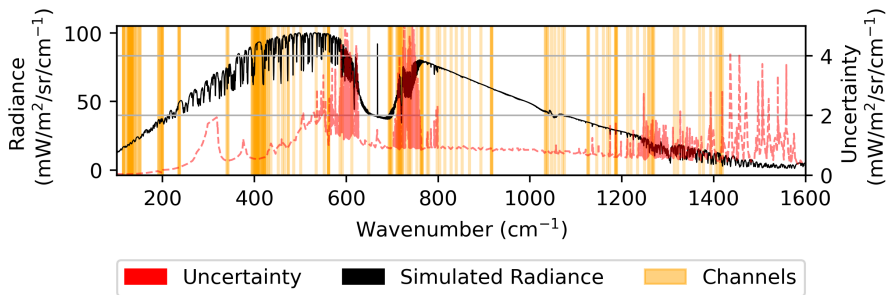
Figure 9. The uncertainty used for FORUM-aircraft configurations is overlaid on an example simulated upwelling spectrum at the altitude of the higher SLR. This is composed of the instrument uncertainty and the uncertainty that arises from the FORUM apodisation process discussed in Section 6.1. This uncertainty squared is used as the main diagonal of $\mathbf{S_y}$. The instrument uncertainty is the radiometric calibration and random noise for each instrument combined in quadrature for a single TAFTS scan and six ARIES scans. For both instruments, this uncertainty is dominated by the calibration, particularly for ARIES, where the random noise is reduced due to multiple scans. The impact of the FORUM apodisation process can be seen most clearly in the 15 micron CO_2 band and between 1200-1400 cm^{-1}. The 200 channels selected for the aircraft retrievals are also shown.

6.2 Channel Selection and Testing on Simulations

Using the FORUM-aircraft measurement covariance in Figure 9, new channels have been selected to optimise the information content for the FORUM-aircraft configuration using the same approach as in Section 3.2.

The 200 channels with the highest information content are shown in Figure 9 and represent 63% of the total available information content, comparable to the FORUM configuration's channel selection in Section 3. Similar to the FORUM configuration, the FORUM-aircraft configuration selects channels in the 350-500 cm^{-1} region and the 667 cm^{-1} CO_2 band wings despite the larger measurement covariance (compare Figure 9 to Figure 1b). However, as the uncertainty for the FORUM-aircraft configuration is considerably reduced below 200 cm^{-1} relative to the rest of its spectral range, 23% of its channels have been selected in this region while none were identified for the FORUM configuration in this range.

To compare the performance of the FORUM-aircraft against the FORUM configuration, the testing in Section 4.1 has been repeated using the newly selected channels and measurement covariance calculated for the FORUM-aircraft configuration. These FORUM-aircraft retrievals have been performed using the same test cases identified in Section 4 but for an observing sensor at the pressure level of the higher SLR of the C153 flight. A full bias comparison can be seen in the supplementary information, however there is an improvement of up to 2 % and 0.1 K in the water vapour and temperature bias, respectively, against the FORUM configuration below the pressure level of the higher SLR. The median DOFS for temperature was also reduced by ∼0.4 due to the larger measurement covariance in the CO_2 band wings. The similarity between the FORUM-aircraft and FORUM retrieval performance across the test cases hints that when we apply the IMS FORUM-aircraft configuration to real observations in the next section, the results will give a realistic indication of the potential quality of retrievals that can be expected from the FSI.

7 Retrievals from Aircraft Observations

7.1 Initial Retrieval

Retrievals of temperature and water vapour were performed using the approach described in Section 2.1 on the selected aircraft observations (Section 5.2) that have been modified to mimic the FSI's instrument line shape. Retrievals of the spectral surface emissivity and surface skin temperature were also obtained simultaneously and results can be found in the supplementary information. In each case, the closest hourly ERA5 data was used as the a-priori for surface skin temperature, atmospheric temperature, and water vapour, accompanied by the weak, global a-priori covariance outlined in Section 2. The average retrieved surface skin temperature was found to be 280.3 ± 0.2 K across the eight cases consistent with the iterative process used in Warwick et al. (2022).

Figure 10 shows the mean temperature and water vapour retrievals for all eight observations (red curves) colocated with the release of each dropsonde. The black curve shows the average of all the dropsonde measurements with their respective averaging kernel applied. These are referred to as AK-treated dropsonde measurements, $\mathbf{x}_{AK}$, and are calculated using the following equation:
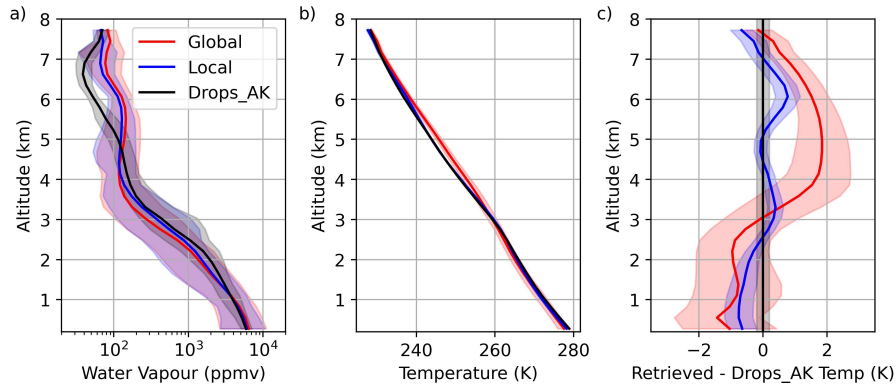
Figure 10. The mean retrieved (a) water vapour and (b) temperature profiles, as well as the (c) residual between the retrieved temperature and each AK-treated dropsonde profile (Drops_AK), using the global and local grid a-priori covariances for temperature in red and blue respectively. The Drops_AK water profile and temperature profiles shown in (a) and (b) did not change significantly with the different covariances and so are shown only for the global covariance. The temperature residuals shown in (c) were calculated with respect to the correct Drops_AK profile. The global a-priori covariance is calculated from ERA5 temperatures across the globe for three days as used in Trent et al. (2023). The local a-priori covariance is calculated from ERA5 temperatures surrounding the SLRs for the duration of the flight. Blue and red shaded regions show the full spread of retrieved profiles with purple regions showing the overlap. The black shaded region in (a) shows the full spread of AK-treated dropsonde profiles as well as the measurement uncertainty, and in (b) and (c) shows the dropsonde measurement uncertainty only.

$$\mathbf{x}_{\mathrm{AK}} = \mathbf{x}_a + \mathbf{A}(\mathbf{x} - \mathbf{x}_a) \tag{6}$$

where the averaging kernel used is calculated for each individual retrieval.

The water vapour retrieval captures the AK-treated dropsonde profile below approximately 5 km within its uncertainty. However, the temperature retrieval has a limited performance, particularly above 4 km and near the surface, with a mean retrieval bias of up to 2 K.

Warwick et al. (2022) indicated the ARIES spectra were, at best, poorly constrained in regions of the spectrum sensitive to atmospheric temperature due to possible heating of the instrument housing. Here, the additional impact of the apodisation in the CO_2 band on the measurement exacerbates this unreliable information and results in the large temperature residuals between the AK-treated dropsonde and retrieved profiles as the retrieval attempts to fit anomalously warm observations. It is unlikely this is due to the dropsondes' representation of the state. While Figure 7b shows a variation of up to 0.5 K in ERA5 around each of the dropsondes between 4 and 7 km, a systematic effect is observed across all of the retrievals.

To compensate for this, the a-priori covariance for temperature has been tightened to the local covariance of ERA5 temperature profiles surrounding the SLRs for the duration of the flight. The a-priori covariance for water vapour has not been tightened and is still derived from global ERA5 data across three days. The impact on the mean temperature and water vapour
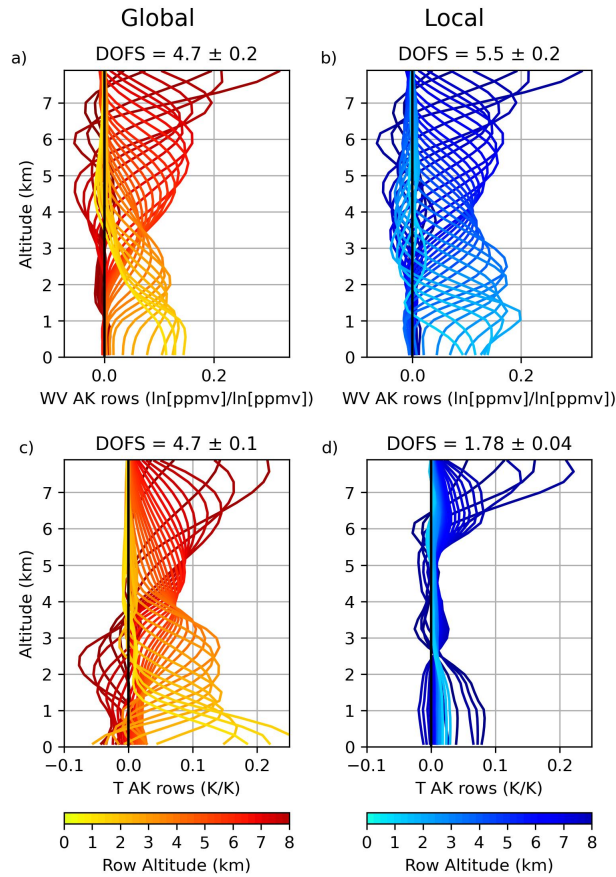
Figure 11. Rows of the mean averaging kernels (AK) for **(a)-(b)** water vapour and **(c)-(d)** temperature calculated from retrievals of the C153 observations with colours representing the dropsonde altitude of each profile level. **(a)** and **(c)** follow the same colour scheme and are the rows of the AKs when the a-priori temperature covariance was derived from three days of global ERA5. **(b)** and **(d)** follow the same colour scheme and are the rows of the AKs when the a-priori temperature covariance was derived from the ERA5 surrounding the SLRs for the duration of the flight. The water vapour a-priori covariance used is the same in both sets of retrievals. The mean and standard deviation of the respective DOFS from the eight retrievals are shown for each plot.
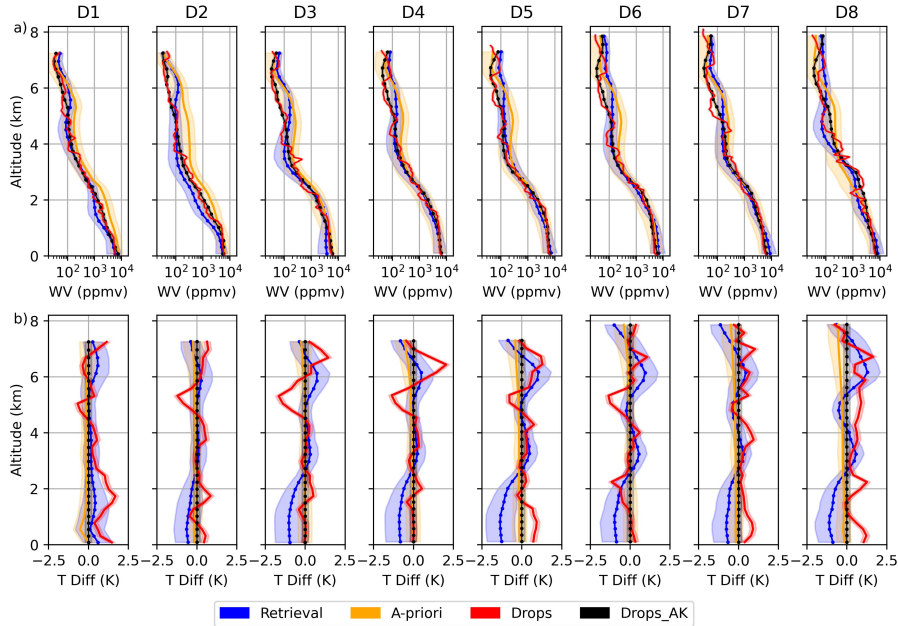
Figure 12. (a) Water vapour retrievals and (b) the difference between the retrieved temperature and AK-treated dropsonde profiles performed using the FORUM-aircraft radiances. The shaded region in each retrieved value represents two ESD of the retrieval derived from the square-root diagonal of $\mathbf{S_x}$. The a-priori is shown in orange with the shaded region showing the a-priori standard deviation. The dropsonde profiles from each case are shown in red, and each one has had their respective averaging kernels (Drops_AK) applied which are shown in black. The shading around the dropsonde and Drops_AK profiles represents the uncertainties outlined in Section 5.1.2. For temperature, the dropsonde uncertainty is represented as 0.2 K. For water vapour, the dropsonde uncertainty varies with altitude but remains below 9%.

AKs across the 8 cases is shown in Figure 11. As expected, Figure 11d shows a reduction in the temperature AKs, with a 60% reduction in the average temperature DOFS. This tightening of the a-priori temperature covariance also leads to an increase in the water vapour AKs focused below 4 km with a 17% increase in the water vapour DOFS in Figure 11b.

Figure 10 shows that the implementation of the local temperature constraint significantly improves agreement between the temperature retrievals (blue curve) and the AK-treated dropsonde profiles, with a mean temperature residual of at most 0.8 K. A similar improvement is observed in the percentage difference between the water vapour retrievals and AK-treated dropsonde, with an improvement of up to 20% at 3 km, and up to 33% at 6km. A smaller effect is observed in the retrievals at higher altitudes. This method enables the joint retrieval of temperature, water vapour, surface emissivity, and surface skin temperature that was not possible in Warwick et al. (2022) due to the limitations outlined for the ARIES spectra.

7.2 Revised Retrievals

Given the findings in Section 7.1, we focus on the retrievals performed using the local a-priori covariance for temperature derived from ERA5 temperature profiles surrounding the SLRs for the duration of the flight, and the global a-priori covariance
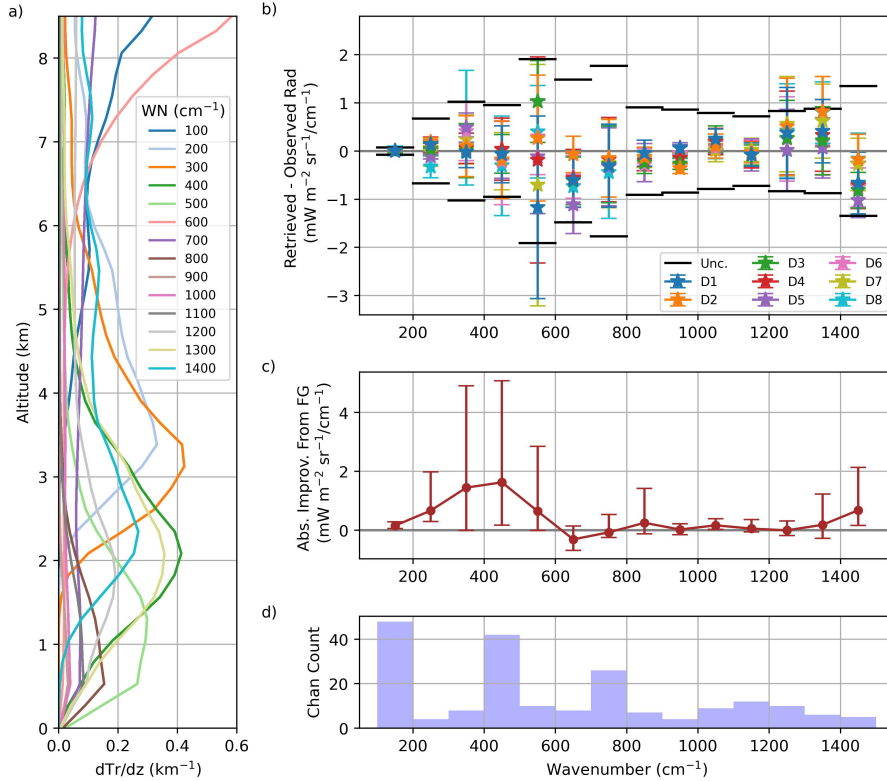
Figure 13. (a) The mean weighting function (change in transmission (Tr) with altitude (z)) for each wavenumber (WN) bin averaged across the 200 selected channels for all 8 dropsondes. (b) The radiance residuals in the selected 200 channels between the retrieved and FORUM-aircraft observed spectra for all cases. Residuals have been averaged over $100 \, \mathrm{cm}^{-1}$ bins in and shown is the mean and standard deviation for the bin. The black line represents the mean uncertainty (Unc.) from Figure 9, which is the square-root diagonal of $\mathbf{S_y}$, in that bin. (c) The mean absolute improvement in the spectral residual from the first guess (FG) spectra to the retrieved spectra across all 8 cases in each bin. Error bars show the minimum and maximum values across the 8 cases in each bin. (d) The number of channels in each bin.

for skin temperature and water vapour. The surface emissivity a-priori covariance is derived from the UWIREMIS atlas for sea surface types, and using the Huang emissivity atlas for land surface types, as outlined in Section 3.1.

Figure 12 shows each retrieved water vapour and temperature profile compared to the a-priori, and the reference AK-treated
430 and untreated dropsonde profiles. Retrievals of water vapour typically bring the a-priori estimate closer to the AK-treated dropsonde profile. This is reflected by an 18% reduction in the RMSE relative to AK-treated dropsonde profiles throughout the vertical profile (Table 3). Retrievals of temperature have a restricted movement from the a-priori as outlined in Section 7.1, and as a result applying the AKs in Figure 11d brings each dropsonde profile to within 0.6 K of their corresponding a-priori.

Both the retrievals of temperature and water vapour generally capture their reference state within their uncertainty. However,
435 some issues are apparent: for example, the water vapour retrievals struggle with a persistently dry layer measured by the

Table 3. The RMSE value relative to each AK-treated dropsonde profile for temperature and water vapour for the 8 observations against the a-priori (ERA5) and retrieved profiles. RMSE values have been separated into above and below 5 km

	A-priori	Retrieval
Full T (K)	0.21	0.57
Full WV (log(kg/kg))	0.50	0.41
Below 5 km T (K)	0.15	0.59
Above 5 km T (K)	0.29	0.53
Below 5 km WV (log(kg/kg))	0.41	0.30
Above 5 km WV (log(kg/kg))	0.65	0.57

dropsondes between 5 and 7 km; and the temperature retrievals generally have a warm bias above 5 km, and a cold bias closer to the surface. A deeper analysis of the retrievals follows, divided into altitudes above and below 5 km. To aid this analysis, Figure 13 shows the (a) average weighting function for selected $100 \, \mathrm{cm}^{-1}$ wavenumber bands, (b) spectral residuals between the final retrieved state and the observations, and (c) the improvement in the residuals relative to the original from the a-priori.

7.2.1 Above 5km

Figure 12a shows that the retrieved water vapour concentration is generally overestimated relative to the dropsonde measurements at altitudes above 5 km. The most obvious discrepancy occurs in a layer between approximately 5 and 7 km, where the dropsondes are persistently drier than the a-priori estimate. Although, in most cases, the retrieved profiles (blue lines) move towards the corresponding AK-treated dropsonde profiles (black lines) between 5 and 6 km, the shift is small and the difference between them can exceed 2 ESDs of the retrieval. Above 6 km, movement from the a-priori towards the AK-treated dropsonde is less obvious.

As the AK-treated dropsonde also does not deviate substantially from the original dropsonde profile in this region, it is not expected that these differences are caused by a weak sensitivity to the profile or the a-priori. Figure 13a shows the channels with the highest sensitivity between 5 and 7 km tend to be clustered between 100 and $400 \, \mathrm{cm}^{-1}$ and above $1400 \, \mathrm{cm}^{-1}$, within the water vapour rotation and vibrational-rotation bands. Between 100 and $400 \, \mathrm{cm}^{-1}$ water vapour spectroscopy, including line and continuum contributions, has been continuously updated over the last couple of decades but is still subject to relatively large uncertainty (Mlawer et al., 2019, 2023), which will contribute to forward model error. Above $1400 \, \mathrm{cm}^{-1}$ the fitted radiances are on average underestimated by $-0.6 \, \mathrm{mWm}^{-2}\mathrm{sr}^{-1}/\mathrm{cm}^{-1}$, however this remains within the measurement covariance (Figure 13b).

The temperature retrievals broadly capture the AK-treated dropsonde within the uncertainty of the retrieval but generally do not present an improvement from the a-priori. As discussed in Section 7.1, an overestimation of up to 1.3 K is seen above

5 km due to the ARIES spectra. However, there is also an underestimation observed closer to the aircraft. In Warwick et al. (2022), there were notable differences between simulated radiances and ARIES observations between 650 and 700 cm^{-1}. Six out of the eight channels in the 600-700 cm^{-1} bin are within this spectral range. As Figure 13a shows, the channels used within this bin show a greater sensitivity to the atmosphere above 7 km, and the fitted radiances within this bin are generally underestimated (Figure 13b).

7.2.2 Below 5km

When making comparisons to the dropsonde profiles at lower altitudes, it is important to note that the dropsondes have travelled up to 23 km from their release when they reach the surface. This is most significant for the retrievals closest to dropsonde 1 and 7 where the radiometric observations are taken over a minute from the dropsonde releases and so have a weaker reference of the atmospheric state at lower altitudes. Furthermore, the ERA5 reanalyses surrounding each dropsonde in Figure 7 imply a higher variability in the water vapour concentrations between 2 and 4 km, reaching up to 30% in water vapour for dropsonde 2. The corresponding temperature standard deviation reaches up to 0.5 K closer to the surface for all dropsondes. Hence it is feasible that the dropsonde profiles are less representative of the atmosphere sounded by the aircraft spectrometers at these altitudes.

Nonetheless, below 5 km the a-priori for water vapour for dropsondes 3-7 is close to the dropsonde profile, particularly below 2 km. For dropsondes 1, 2, and 8, there is a larger discrepancy that the retrieval successfully reduces, shifting the retrieved values closer to the relevant AK-treated dropsonde profile. Indeed, in all cases except dropsonde 2, the retrieval uncertainty fully encompasses the dropsonde values below 4 km. Even for the case closest to dropsonde 2, the retrieval significantly shifts from the a-priori closer to the dropsonde profile, with the largest spectral shifts observed between 200 and 600 cm^{-1} (Figure 13b).

Between 2 and 5 km, all the temperature retrievals capture the AK-treated dropsonde profile within their retrieval uncertainty with limited movement from the a-priori as would be expected from the AKs (Figure 11d). Nearer the surface, the average retrieval bias for the retrievals closest to dropsondes 2-8 is -0.9±0.2 K relative to the AK-treated dropsonde profiles. Of these cases only the retrieval closest to dropsonde 5 underestimates the AK-treated dropsonde temperature outside of both their uncertainties, and this by only 0.1 K. The retrieval closest to dropsonde 1 is the only case that shows a warm bias to the AK-treated dropsonde profile nearer the surface, however as previously mentioned, in this instance the dropsonde provides a weaker reference of the true profile.

These temperature and humidity changes are manifested in radiance space as shown in Figure 13b. Figure 13a highlights that the spectral regions between 400 and 600 cm^{-1} and 1200 and 1400 cm^{-1} are most sensitive to lower altitudes, particularly below 3 km. In these bins, particularly in the far-infrared, the retrieval reduces the spectral residuals by up to 5 $mWm^{-2}sr^{-1}/cm^{-1}$ from the first guess spectra (Figure 13c). Despite these improvements, the retrievals closest to dropsondes 1-3 still demonstrate a limited fit in the 500-600 cm^{-1} and 1300-1400 cm^{-1} bins. While the timing of dropsonde 1 is somewhat offset from the radiometric aircraft measurements the same is not true for dropsondes 2 and 3. Dropsondes 1 and

490   2 also show enhanced water vapour variability between 3 and 4 km in the surrounding ERA5 profiles compared to the other cases (Figure 7b), but this enhancement is not seen around dropsonde 3.

8   Conclusions

We present the extension of the Infrared Microwave Sounding retrieval scheme into the far-infrared in preparation for the upcoming FORUM mission. Retrievals of temperature and water vapour have been evaluated through a two-stage testing

495   process: on simulated FORUM clear-sky radiances, and on observed clear-sky radiances from the upper troposphere. For the former, we make comparisons to the 'true' profiles used to generate the simulations, while for the latter, we make comparisons to in-situ measurements of the atmospheric state.

For the FORUM configuration, the measurement covariance is based on the expected apodised NESR and target ARA for the FORUM Sounding Instrument. An information content analysis was performed to optimise the channels used in the

500   retrieval, resulting in the selection of 200 channels. The highest channel density was seen in the 400-600 cm^{-1} region due to the sensitivity of radiances to water vapour and temperature coupled with the relatively low NESR and ARA in this region.

The performance of IMS was first assessed using 240 RTTOVv12 simulations of TOA radiances based on MERRA-2 re-analysis profiles. Retrievals using the FORUM configuration had a tighter measurement covariance than the IASI configuration below $\sim$1200 cm^{-1}. Both configurations demonstrated comparable retrieval biases. However, slight improvements in the FO-

505   RUM median retrieval bias were observed in the mid to upper troposphere for water vapour, with a reduced median uncertainty of at most 7 %, and an increase of approximately 1 DOFS for both water vapour and temperature due to additional information in the upper troposphere. We stress that the goal of the comparison is not to assess which instrument is better in terms of their retrieval performance, but rather a sanity check of the new, extended IMS code. In particular, it is worth noting that in this comparison the measurement covariance used for IASI is not the quoted instrument NESR but instead implicitly includes the

510   effects of instrumental and forward model error. For FORUM, the instrumental error has been approximated using the target instrument specifications, and so it is likely that the comparison overstates the improvement that FORUM will bring relative to IASI observations.

Coincident aircraft observations of far and mid-infrared radiances were then used to test IMS on clear-sky cases. These were taken during an aircraft flight in the upper troposphere, with periodic release of dropsondes to measure the atmospheric

515   state. Eight observations closest to each dropsonde release were selected and modified to emulate the FORUM Sounding Instrument's spectral characteristics. The combination of the aircraft and FORUM Sounding instrument characteristics results in an increased spectral uncertainty, particularly in the 15 micron CO_2 absorption band. This propagates through to change the channels selected for the retrievals when compared to the TOA simulation study. Applying this revised 'FORUM-aircraft' configuration to simulated radiances aircraft level radiances from the MERRA-2 test set shows only a limited impact on the

520   retrieved temperature and water vapour profiles compared to values derived using the original 'FORUM' configuration from the equivalent TOA radiances. This gives confidence that the results obtained here from the aircraft observations are indicative of what might be expected from FORUM when it is operating.

Retrievals of the FORUM-aircraft observations required the a-priori covariance for temperature to be tightened to the local ERA5 grid of the SLRs for the duration of the flight due to the larger measurement uncertainty associated with the observed spectra, particularly across the 15 micron CO_2 band. This enabled simultaneous retrievals of temperature and water vapour, exploiting the full FSI spectral range. Tightening this constraint had the additional benefit of reducing the bias in the water vapour retrieval by up to 33%. The final retrievals of temperature and water vapour generally captured the dropsonde measurements of the atmospheric state, with the RMSE in water vapour concentration reducing by 18% from the a-priori to the retrieved state across all eight cases. We note that the results do still highlight some inconsistencies, with both the ERA-5 a-priori and retrievals consistently overestimating the humidity between 5 and 7 km, and a persistent cold bias below 2 km in seven out of the eight cases analysed. These deficiencies are manifested in the radiance residuals seen in the final, fitted spectra and we use these to postulate that the humidity bias may be related to water vapour spectroscopic uncertainty in the far-infrared. While our analysis implies that the variability around each dropsonde is relatively small, the near surface bias may be partly related to the dropsonde drift away from the aircraft as it descends through the atmosphere.

To summarise, the IMS scheme has been extended to cover the far-infrared spectral range in preparation for the FORUM mission. It has now been tested on multiple aircraft-level observations of upwelling far-infrared radiances, as well as a diverse set of TOA simulated upwelling radiances, exploiting channels from the full FORUM spectral range. Pending the real FORUM Sounding Instrument systematic and random uncertainties, IMS is ready to use for clear-sky retrievals from the FORUM Sounding Instrument.

Data availability. The ERA5 data is from the Copernicus Climate Change Service (C3S) Climate Data Store (CDS). The MERRA-2 data is from the NASA GMAO website. The TAFTS and ARIES observations can be found on the CEDA archive.

Author contributions. The study design was conceived by SP, HEB, and CC. SP extended the retrieval framework, conducted the validation work, and wrote the first draft of the manuscript. HEB, CC, and RS provided expertise and contributed to discussions of the results and revisions of the manuscript. JEM and LW took the measurements from the TAFTS instrument as part of the PIKNMIX-F campaign, and provided expertise on the TAFTS observations. SF provided the ARIES data.

Competing interests. The authors declare that they have no conflict of interest.

Acknowledgements. SP was funded by NERC under Grant No. NE/S007415/1 via the SSCP DTP. HB was funded as part of NERC's support of the National Centre for Earth Observation under Grant No. NE/R016518/1. The PIKNMIX-F flight campaign was jointly funded by the Met Office and the ESA. Airborne data was obtained using the BAe-146- 301 Atmospheric Research Aircraft flown by Airtask Ltd and

550 managed by FAAM Airborne Laboratory, now jointly operated by UKRI and the University of Leeds. The authors would like to thank the instrument operators, aircrew, operations staff, and engineers for their support during the campaign.

References

Allan, R. P., Willett, K. M., John, V. O., and Trent, T.: Global Changes in Water Vapor 1979–2020, Journal of Geophysical Research: Atmospheres, 127, https://doi.org/10.1029/2022jd036728, 2022.

Andrews, D. G.: An introduction to atmospheric physics, Cambridge University Press, Cambridge, England, 2000.

Arshad, M., Ma, X., Yin, J., Ullah, W., Liu, M., and Ullah, I.: Performance evaluation of ERA-5, JRA-55, MERRA-2, and CFS-2 reanalysis datasets, over diverse climate regions of Pakistan, Weather and Climate Extremes, 33, https://doi.org/10.1016/j.wace.2021.100373, 2021.

Brindley, H. E. and Harries, J. E.: The impact of far i.r. absorption on clear sky greenhouse forcing: sensitivity studies at high spectral resolution, Journal of Quantitative Spectroscopy and Radiative Transfer, 60, 151–180, https://doi.org/10.1016/S0022-4073(97)00152-0, 1998.

Canas, T. A., Murray, J. E., and Harries, J. E.: Tropospheric Airborne Fourier transform spectrometer (TAFTS), Satellite Remote Sensing of Clouds and the Atmosphere II, 3220, 91 – 102, https://doi.org/10.1117/12.301139, 1997.

Chahine, M. T., Pagano, T. S., Aumann, H. H., Atlas, R., Barnett, C., Blaisdell, J., Chen, L., Divakarla, M., Fetzer, E. J., Goldberg, M., Gautier, C., Granger, S., Hannon, S., Irion, F. W., Kakar, R., Kalnay, E., Lambrigtsen, B. H., Lee, S., Le Marshall, J., Mcmilan, W. W., Mcmillin, L., Olsen, E. T., Revercomb, H., Rosenkranz, P., Smith, W. L., Staelin, D., Strow, L. L., Susskind, J., Tobin, D., Wolf, W., and Zhou, L.: AIRS: Improving Weather Forecasting and Providing New Data on Greenhouse Gases, Bulletin of the American Meteorological Society, 87, 911–926, https://doi.org/10.1175/bams-87-7-911, 2006.

Chevallier, F., Michele, S. D., and McNally, A.: Diverse profile datasets from the ECMWF 91-level short-range forecasts, Tech. Rep. December, ECMWF, https://www.ecmwf.int/node/8685, 2006.

Chung, E.-S., Soden, B., Sohn, B. J., and Shi, L.: Upper-tropospheric moistening in response to anthropogenic warming, Proceedings of the National Academy of Sciences, 111, 11 636–11 641, https://doi.org/10.1073/pnas.1409659111, 2014.

Clough, S., Shephard, M., Mlawer, E., Delamere, J., Iacono, M., Cady-Pereira, K., Boukabara, S., and Brown, P.: Atmospheric radiative transfer modeling: a summary of the AER codes, Journal of Quantitative Spectroscopy and Radiative Transfer, 91, 233–244, https://doi.org/10.1016/j.jqsrt.2004.05.058, 2005.

Collard, A. D.: Selection of IASI Channels for Use in Numerical Weather Prediction Selection of IASI Channels for Use in Numerical Weather Prediction, Tech. rep., ECMWF, http://www.ecmwf.int/publications/, 2007.

Dessler, A. E., Zhang, Z., and Yang, P.: Water-vapor climate feedback inferred from climate fluctuations, 2003–2008, Geophysical Research Letters, 35, https://doi.org/10.1029/2008GL035333, 2008.

Di Natale, G., Palchetti, L., Bianchini, G., and Ridolfi, M.: The two-stream δ-Eddington approximation to simulate the far infrared Earth spectrum for the simultaneous atmospheric and cloud retrieval, Journal of Quantitative Spectroscopy and Radiative Transfer, 246, 106 927, https://doi.org/10.1016/j.jqsrt.2020.106927, 2020.

Dirksen, R. J., Sommer, M., Immler, F. J., Hurst, D. F., Kivi, R., and Vömel, H.: Reference quality upper-air measurements: GRUAN data processing for the Vaisala RS92 radiosonde, Atmospheric Measurement Techniques, 7, 4463–4490, https://doi.org/10.5194/amt-7-4463-2014, 2014.

Ferreira, A. P., Nieto, R., and Gimeno, L.: Completeness of radiosonde humidity observations based on the Integrated Global Radiosonde Archive, Earth System Science Data, 11, 603–627, https://doi.org/10.5194/essd-11-603-2019, 2019.

Fetzer, E. J., Read, W. G., Waliser, D., Kahn, B. H., Tian, B., Vömel, H., Irion, F. W., Su, H., Eldering, A., de la Torre Juarez, M., Jiang, J., and Dang, V.: Comparison of upper tropospheric water vapor observations from the Microwave Limb Sounder and Atmospheric Infrared Sounder, Journal of Geophysical Research: Atmospheres, 113, https://doi.org/10.1029/2008jd010000, 2008.

590 Gelaro, R., McCarty, W., Suárez, M. J., Todling, R., Molod, A., Takacs, L., Randles, C. A., Darmenov, A., Bosilovich, M. G., Reichle, R., Wargan, K., Coy, L., Cullather, R., Draper, C., Akella, S., Buchard, V., Conaty, A., da Silva, A. M., Gu, W., Kim, G.-K., Koster, R., Lucchesi, R., Merkova, D., Nielsen, J. E., Partyka, G., Pawson, S., Putman, W., Rienecker, M., Schubert, S. D., Sienkiewicz, M., and Zhao, B.: The Modern-Era Retrospective Analysis for Research and Applications, Version 2 (MERRA-2), Journal of Climate, 30, 5419–5454, https://doi.org/10.1175/jcli-d-16-0758.1, 2017.

595 Global Modeling and Assimilation Office and Pawson, S.: MERRA-2 inst3_3d_asm_Np: 3d,3-Hourly, Instantaneous, Pressure-Level, Assimilation, Assimilated Meteorological Fields V5.12.4, https://gmao.gsfc.nasa.gov/reanalysis/MERRA-2/, 2015a.

Global Modeling and Assimilation Office and Pawson, S.: MERRA-2 inst1_2d_asm_Nx: 2d,3-Hourly, Instantaneous, Single-Level, Assimilation, Single-Level Diagnostics V5.12.4, https://gmao.gsfc.nasa.gov/reanalysis/MERRA-2/, 2015b.

Haiden, T., Janousek, M., Bidlot, J., Buizza, R., Ferranti, L., Prates, F., and Vitart, F.: Evaluation of ECMWF forecasts, including the 2018
600 upgrade, European Centre for Medium Range Weather Forecasts Reading, UK, https://doi.org/10.21957/ldw15ckqi, 2018.

Hale, G. M. and Querry, M. R.: Optical Constants of Water in the 200-nm to 200-m Wavelength Region, Applied Optics, 12, 555, https://doi.org/10.1364/ao.12.000555, 1973.

Harries, J., Carli, B., Rizzi, R., Serio, C., Mlynczak, M., Palchetti, L., Maestri, T., Brindley, H., and Masiello, G.: The far-infrared Earth, Reviews of Geophysics, 46, https://doi.org/10.1029/2007RG000233, 2008.

605 Harries, J. E.: The greenhouse Earth: A view from space, Quarterly Journal of the Royal Meteorological Society, 122, 799–818, https://doi.org/10.1002/qj.49712253202, 1996.

Hilton, F., Armante, R., August, T., Barnet, C., Bouchard, A., Camy-Peyret, C., Capelle, V., Clarisse, L., Clerbaux, C., Coheur, P.-F., Collard, A., Crevoisier, C., Dufour, G., Edwards, D., Faijan, F., Fourrié, N., Gambacorta, A., Goldberg, M., Guidard, V., Hurtmans, D., Illingworth, S., Jacquinet-Husson, N., Kerzenmacher, T., Klaes, D., Lavanant, L., Masiello, G., Matricardi, M., McNally, A., Newman, S., Pavelin, E.,
610 Payan, S., Péquignot, E., Peyridieu, S., Phulpin, T., Remedios, J., Schlüssel, P., Serio, C., Strow, L., Stubenrauch, C., Taylor, J., Tobin, D., Wolf, W., and Zhou, D.: Hyperspectral Earth Observation from IASI: Five Years of Accomplishments, Bulletin of the American Meteorological Society, 93, 347–370, https://doi.org/10.1175/bams-d-11-00027.1, 2012.

Huang, L., Mo, Z., Liu, L., Zeng, Z., Chen, J., Xiong, S., and He, H.: Evaluation of Hourly PWV Products Derived From ERA5 and MERRA-2 Over the Tibetan Plateau Using Ground-Based GNSS Observations by Two Enhanced Models, Earth and Space Science, 8,
615 https://doi.org/10.1029/2020EA001516, 2021.

Huang, X., Chen, X., Zhou, D. K., and Liu, X.: An observationally based global band-by-band surface emissivity dataset for climate and weather simulations, Journal of the Atmospheric Sciences, 73, 3541–3555, https://doi.org/10.1175/JAS-D-15-0355.1, 2016.

IPCC: The Earth's Energy Budget, Climate Feedbacks and Climate Sensitivity, p. 923–1054, Cambridge University Press, 2023.

Jiang, J. H., Su, H., Zhai, C., Wu, L., Minschwaner, K., Molod, A. M., and Tompkins, A. M.: An assessment of upper troposphere and
620 lower stratosphere water vapor in MERRA, MERRA2, and ECMWF reanalyses using Aura MLS observations, Journal of Geophysical Research, 120, 11,468–11,485, https://doi.org/10.1002/2015JD023752, 2015.

Johnston, B. R., Randel, W. J., and Sjoberg, J. P.: Evaluation of tropospheric moisture characteristics among COSMIC-2, ERA5, and MERRA-2 in the tropics and subtropics, Remote Sensing, 13, 1–20, https://doi.org/10.3390/rs13050880, 2021.

Kursinski, E. R. and Gebhardt, T.: A Method to Deconvolve Errors in GPS RO-Derived Water Vapor Histograms, Journal of Atmospheric and Oceanic Technology, 31, 2606–2628, https://doi.org/10.1175/jtech-d-13-00233.1, 2014.

L'Ecuyer, T. S., Drouin, B. J., Anheuser, J., Grames, M., Henderson, D. S., Huang, X., Kahn, B. H., Kay, J. E., Lim, B. H., Mateling, M., Merrelli, A., Miller, N. B., Padmanabhan, S., Peterson, C., Schlegel, N.-J., White, M. L., and Xie, Y.: The Polar Radiant Energy in the Far Infrared Experiment: A New Perspective on Polar Longwave Energy Exchanges, Bulletin of the American Meteorological Society, 102, E1431 – E1449, https://doi.org/10.1175/BAMS-D-20-0155.1, 2021.

Marquardt, D. W.: An Algorithm for Least-Squares Estimation of Nonlinear Parameters, Journal of the Society for Industrial and Applied Mathematics, 11, 431–441, https://doi.org/10.1137/0111030, 1963.

Masuda, K.: Infrared sea surface emissivity including multiple reflection effect for isotropic Gaussian slope distribution model, Remote Sensing of Environment, 103, 488–496, https://doi.org/10.1016/j.rse.2006.04.011, 2006.

Merrelli, A. and Turner, D. D.: Comparing information content of upwelling far-infrared and midinfrared radiance spectra for clear atmosphere profiling, Journal of Atmospheric and Oceanic Technology, 29, 510–526, https://doi.org/10.1175/JTECH-D-11-00113.1, 2012.

Miloshevich, L. M., Vömel, H., Whiteman, D. N., and Leblanc, T.: Accuracy assessment and correction of Vaisala RS92 radiosonde water vapor measurements, Journal of Geophysical Research, 114, https://doi.org/10.1029/2008jd011565, 2009.

Mlawer, E., Cady-Pereira, K., Mascio, J., and Gordon, I.: The inclusion of the MT_CKD water vapor continuum model in the HITRAN molecular spectroscopic database, Journal of Quantitative Spectroscopy and Radiative Transfer, 306, 108 645, https://doi.org/10.1016/j.jqsrt.2023.108645, 2023.

Mlawer, E. J., Turner, D. D., Paine, S. N., Palchetti, L., Bianchini, G., Payne, V. H., Cady-Pereira, K. E., Pernak, R. L., Alvarado, M. J., Gombos, D., Delamere, J. S., Mlynczak, M. G., and Mast, J. C.: Analysis of Water Vapor Absorption in the Far-Infrared and Submillimeter Regions Using Surface Radiometric Measurements From Extremely Dry Locations, Journal of Geophysical Research: Atmospheres, 124, 8134–8160, https://doi.org/10.1029/2018JD029508, 2019.

NOAA ESRL GML CCGG Group: Earth system research laboratory carbon cycle and greenhouse gases group flask-air sample measurements of CH4 at global and regional background sites, 1967-present, 2019a.

NOAA ESRL GML CCGG Group: Earth system research laboratory carbon cycle and greenhouse gases group flask-air sample measurements of CO2 at global and regional background sites, 1967-present, 2019b.

NOAA ESRL GML CCGG Group: Earth system research laboratory carbon cycle and greenhouse gases group flask-air sample measurements of N2O at global and regional background sites, 1967-present, 2019c.

Palchetti, L., Brindley, H., Bantges, R., Buehler, S. A., Camy-Peyret, C., Carli, B., Cortesi, U., Bianco, S. D., Natale, G. D., Dinelli, B. M., Feldman, D., Huang, X. L., C.-Labonnote, L., Libois, Q., Maestri, T., Mlynczak, M. G., Murray, J. E., Oetjen, H., Ridolfi, M., Riese, M., Russell, J., Saunders, R., and Serio, C.: FORUM: unique far-infrared satellite observations to better understand how Earth radiates energy to space, American Meteorological Society, 101, 2030–2046, https://doi.org/10.1175/BAMS-D-19-0322.1, 2020.

Platnick, S., King, M. D., Ackerman, S. A., Menzel, W. P., Baum, B. A., Riédi, J. C., and Frey, R. A.: The MODIS cloud products: Algorithms and examples from Terra, IEEE Transactions on geoscience and Remote Sensing, 41, 459–473, https://doi.org/10.1109/TGRS.2002.808301, 2003.

Ridolfi, M., Bianco, S. D., Roma, A. D., Castelli, E., Belotti, C., Dandini, P., Di Natale, G., Dinelli, B. M., Labonnote, L. C., and Palchetti, L.: FORUM Earth Explorer 9: Characteristics of Level 2 Products and Synergies with IASI-NG, Remote Sensing, 12, 1496, https://doi.org/10.3390/rs12091496, 2020.

Rodgers, C. D.: Inverse Methods for Atmospheric Sounding, vol. 2, World Scientific Publishing, https://doi.org/10.1142/3171, 2000.

Santer, B. D., Po-Chedley, S., Mears, C., Fyfe, J. C., Gillett, N., Fu, Q., Painter, J. F., Solomon, S., Steiner, A. K., Wentz, F. J., Zelinka, M. D., and Zou, C.-Z.: Using Climate Model Simulations to Constrain Observations, Journal of Climate, 34, 6281–6301, https://doi.org/10.1175/jcli-d-20-0768.1, 2021.

665 Saunders, R., Hocking, J., Rundle, D., Rayer, P., Havemann, S., Matricardi, M., Geer, A., Lupu, C., Brunel, P., and Vidot, J.: RTTOV-12 Science and Validation Report, Tech. rep., EUMETSAT, https://nwp-saf.eumetsat.int/site/download/documentation/rtm/docs_rttov12/rttov12_svr.pdf, 2017.

Schröder, M., Lockhoff, M., Shi, L., August, T., Bennartz, R., Brogniez, H., Calbet, X., Fell, F., Forsythe, J., Gambacorta, A., Ho, S.-p., Kursinski, E. R., Reale, A., Trent, T., and Yang, Q.: The GEWEX Water Vapor Assessment: Overview and Introduction to Results and

670 Recommendations, Remote Sensing, 11, https://doi.org/10.3390/rs11030251, 2019.

Seeman, S., Borbas, E. E., Knuteson, R., Stephenson, G. R., and Huang, H.: Development of a Global Infrared Land Surface Emissivity Database for Application to Clear Sky Sounding Retrievals from Multispectral Satellite Radiance Measurements, Journal of Applied Meteorology and Climatology, 47, 108–123, https://doi.org/10.1175/2007jamc1590.1, 2008.

Shi, L., Schreck III, C. J., John, V. O., Chung, E.-S., Lang, T., Buehler, S. A., and Soden, B. J.: Assessing the consistency of satellite-

675 derived upper tropospheric humidity measurements, Atmospheric Measurement Techniques, 15, 6949–6963, https://doi.org/10.5194/amt-15-6949-2022, 2022.

Siddans, R.: Water Vapour Climate Change Initiative (WV_cci) - Phase One, Deliverable 2.2; Version 1.0, RAL Space Remote Sensing Group-Technical Report, Tech. rep., RAL Space, https://climate.esa.int/documents/2497/Water_Vapour_CCI_D2.2_ATBD_Part2-IMS_L2_product_v2.0.pdf, 2019.

680 Siddans, R., Knappett, D., Kerridge, B., Waterfall, A., Hurley, J., Latter, B., Boesch, H., and Parker, R.: Global height-resolved methane retrievals from the Infrared Atmospheric Sounding Interferometer (IASI) on MetOp, Atmospheric Measurement Techniques, 10, 4135–4164, https://doi.org/10.5194/amt-10-4135-2017, 2017.

Sinha, A. and Harries, J. E.: Water vapour and greenhouse trapping: The role of far infrared absorption, Geophysical Research Letters, 22, 2147–2150, https://doi.org/10.1029/95GL01891, 1995.

685 Sun, B., Calbet, X., Reale, A., Schroeder, S., Bali, M., Smith, R., and Pettey, M.: Accuracy of Vaisala RS41 and RS92 upper tropospheric humidity compared to satellite hyperspectral infrared measurements, Remote Sensing, 13, 173, https://doi.org/10.3390/rs13020173, 2021.

Trent, T., Schröder, M., and Remedios, J.: GEWEX Water Vapor Assessment: Validation of AIRS Tropospheric Humidity Profiles With Characterized Radiosonde Soundings, Journal of Geophysical Research: Atmospheres, 124, 886–906, https://doi.org/10.1029/2018jd028930, 2019.

690 Trent, T., Siddens, R., Kerridge, B., Schroeder, M., Scott, N. A., and Remedios, J.: Evaluation of tropospheric water vapour and temperature profiles retrieved from Metop-A by the Infrared and Microwave Sounding scheme, Atmospheric Measurement Techniques, https://doi.org/10.5194/amt-16-1503-2023, 2023.

Warwick, L., Brindley, H., Roma, A. D., Fox, S., Havemann, S., Murray, J., Oetjen, H., Price, H. C., Schüttemeyer, D., Sgheri, L., and Tiddeman, D. A.: Retrieval of Tropospheric Water Vapor From Airborne Far-Infrared Measurements: A Case Study, Journal of Geophysical

695 Research: Atmospheres, 127, https://doi.org/10.1029/2020jd034229, 2022.

Watson, P.: Progress towards the Implementation of Correlated Observation Errors in 4D-Var, met Office, 2011.

Wilson, S. H. S., Atkinson, N. C., and Smith, J. A.: The Development of an Airborne Infrared Interferometer for Meteorological Sounding Studies, Journal of Atmospheric and Oceanic Technology, 16, 1912–1927, https://doi.org/10.1175/1520-0426(1999)016<1912:tdoaai>2.0.co;2, 1999.